Effects of swirler vane angle on palm biodiesel/natural gas combustion in swirl-stabilised gas turbine combustor

Meng-Choung Chiong[a,*], Agustin Valera-Medina[b], William Woei Fong Chong[a], Cheng Tung Chong[c], Guo Ren Mong[a], Mohammad Nazri Mohd Jaafar[a]

[a] *School of Mechanical Engineering, Faculty of Engineering, Universiti Teknologi Malaysia, 81310 Skudai, Johor, Malaysia*
[b] *College of Physical Sciences and Engineering, Cardiff University, Wales, UK*
[c] *China-UK Low Carbon College, Shanghai Jiao Tong University, Lingang, Shanghai, 201306, China*

Abstract

Combustion characteristics of palm biodiesel/methyl esters (PME) and natural gas (NG) blend were examined using a model gas turbine swirl burner at vane angle (θ) 30°, 45° and 60°. A twin fluid air blast atomiser was utilised for atomising liquid fuel at air-to-liquid ratio (ALR) 2.50. Swirling flow was initiated by using an axial swirler as main air passed through it. Combustible mixture was formed as swirling air flow mixed up with liquid fuel spray at burner outlet. Flame colour for PME/NG was mainly bluish, resembling that of neat PME despite subtle liftoff was observed in PME/NG swirl flames. Flame spectroscopic analysis showed that PME/NG swirl flames were more intense than baseline PME. Furthermore, θ = 60° operation led to significantly lower reaction intensity. Meanwhile, PME/NG combustion with 20%-30% NG input power fraction was observed to lower nitric oxide (NO) emission by a factor of 2.7 when compared with diesel and neat PME in θ = 60° combustion. Novel empirical models for emissions were also proposed, enabling the estimation of NO emission from PME/NG combustion at different NG input power proportions and vane angle. This research shows that PME/NG combustion is a promising way of reducing NO emission against neat PME and diesel in gas turbine operation. Moreover, flame instability provoked by liftoff in dual fuel operation is not aggravated, mainly due to nullification by intensified global reaction when NG is added. Such attributes feature PME/NG as a viable alternative fuel for use in land-based power generation gas turbines.

Keywords: *Dual fuel; Gas turbine; Biodiesel; Natural gas; Swirler vane angle; Emissions*

*Corresponding author
Address: School of Mechanical Engineering, Faculty of Engineering, Universiti Teknologi Malaysia, 81310, Skudai, Johor, Malaysia

Email: mcchiong@outlook.com ; mcchiong2@live.utm.my

1.0 Introduction

The Gas turbine combined cycle (GTCC) has prevailed in conventional coal-fired plants as the most common mean for electricity generation plants in the United States (U.S.) since 2018 [1,2]. Despite coal remaining as the world's major source of energy [3,4], electricity generated by GTCC plants was higher than that of coal-fired power plants by a factor of 1.08 in the U.S. by 2019 [1,2]. The switch from conventional coal-fired plants to GTCC has been a common phenomenon in many developed countries, as reflected by the increase of natural gas (NG) consumption rates in such countries [4–6]. Such transition is mainly due to the characteristic exhaust fumes from coal, which have higher potential to pollute the environment all along the life cycle of this fuel [3]. Moreover, in contrast to conventional coal-fired plants with thermal efficiency of only about 40%, the modern GTCC plants present a thermal efficiency of at least 60% [5]. It was estimated that every 1% increase in thermal efficiency can potentially lead to 50 kilo tons of carbon dioxide (CO_2) reduction in a year [6]. This fact, in conjunction with the development of integrated gasification combined cycles (IGCC) that utilise gas turbines as centerpiece of the plant electricity production, is expected to promote gas turbines as the method of choice for electricity generation in the decades to come [6].

There has been a growing interest in firing gas turbines with liquid biofuels since last decade, with vast majority of published works reported in a recent review [7]. In contrast to fossil fuels, biofuels are renewable, sustainable and potentially carbon neutral. While capacity growth for biofuels remains slow at present, this pattern is expected to increase in the coming decades as biofuels are becoming recognised as viable substitutes for fossil-based energy sources [5]. On this basis, gas turbine manufacturers have delved into fuel-flexible technology, enabling the flexible use of various biofuels in gas turbines [8]. Although biofuels such as bioethanol is highly volatile,

explosive and posing great challenge to the equipment design task [9,10], but most biofuels exhibit inferior physical properties than those of conventional fossil fuels, such as higher flash point, higher viscosity and lower calorific value [7]. This would inherently result in inferior combustion and emissions performance. A possible way of overcoming these biofuels' drawbacks is to utilise the concept of dual fuel combustion. Dual fuel combustion takes in small amounts of secondary fuels to assist the primary biofuel combustion. The increasing demand for biomass-derived alternative fuels has prompted researchers to gain profound understanding on dual fuel combustion characteristics.

Agwu and Valera-Medina [11] noticed an enhanced flame stability and emissions reduction in diesel/syngas co-combustion, when compared with neat diesel at 15 kW input thermal power and equivalence ratio (φ) = 0.7. The NO emissions was lowered by a factor of 1.46 as syngas proportion increased from 10% to 30%. in the diesel/syngas blends. Kurji et al. [12] investigated the effect of methane/CO_2 blend on waste cooking oil biodiesel and diesel combustion using a gas turbine swirl burner. Carbon monoxide (CO) emission was observed to have been lowered by approximately 87% as CO_2 blending ratio increased by 10% on volume basis. Jiang and Agrawal [13] utilised gas turbine swirl burners with a flow-blurring (FB) atomiser to examine methane/glycerol dual fuel combustion. The presence of methane promotes glycerol evaporation rate significantly. This was indicated by CO emissions lower than 40 ppm for co-combustion as compared to those of neat glycerol (>40 ppm). Queiros et al. [14] examined the effect of NG and hydrogen blend on crude glycerol combustion in a model gas turbine swirl burner equipped with an air assisted atomiser. Nitric oxide (NO) emissions from 22/58/20 glycerol/NG/hydrogen combustion were lower than for neat NG by approximately 15 ppm for $\varphi < 1$. Nonetheless, CO emissions from 22/58/20 glycerol/NG/hydrogen combustion were higher than for neat NG by 400

ppm at φ = 0.5. Altaher et al. [15] also studied co-combustion characteristics of biodiesel and NG with model gas turbine swirl burners equipped with a radial swirler. Their study showed that biodiesel/NG combustion resulted in higher NO than for neat NG by averaging 10 ppm from φ = 0.25 to 0.65. In a recent biodiesel/NG co-combustion study, CO from dual fuel combustion at φ = 0.9 was found substantially higher than neat biodiesel and diesel swirl flames owing to the poor fuel-air mixing. Conversely at φ = 0.65, enhanced fuel-air mixing reduces the CO emission but increasing the NO emissions due to the intensified reactions [16]. For the same equivalence ratio range, biodiesel/NG combustion also resulted in higher CO by roughly 60 ppm against NG. It is evident from previous studies that NG is an ideal supplementary fuel for assisting biofuels combustion (recall that methane is the major constituent of NG). This is primarily due to its considerably low prices against that of liquid fuels [17]. On top of this, issues associated with the high-pressure NG tank storage in transportation vehicles is totally resolved for land-based power generation gas turbine applications.

Apart from the dual fuel concept, aerodynamics processes in the combustor are also of prime importance in improving gas turbine combustion. Air swirlers are widely used in gas turbine combustion for generating central recirculating flows that stabilises the flame [18,19]. Central recirculating flows recycles part of the hot combustion product and mixes them with incoming fresh reactant and air, accelerating the rate of reaction and combustion intensity that would, in turns, guarantee flame stabilisation [18,19]. Kim et al. [20,21] examined the effect of swirler vane angle (θ) variation on premixed methane combustion. Despite swirling airflow being desirable for flame stabilisation, excessive increase in vane angle was found exacerbating flame instability. Bhimani et al. [22] studied the effect of swirler vane angle on canola oil and canola oil/methanol blends combustion in a 30 kW cylindrical combustion chamber. It was reported that lower vane

angle undesirably elevated NO_x emissions, owing to the poor fuel/air mixing. Bazooyar et al. [23,24] investigated the effect of vane angle on biodiesel emissions using a semi-industrial boiler. They found that increasing the vane angle from 30° to 45° resulted in 7% NO reduction for 22 bar fuel atomising pressure. Nonetheless, increasing the vane angle from 45° to 60° gave rise to the NO emission surprisingly in their study. Ti et al. [25] reported that flue gas temperature increased by approximately 30% as swirler vane angle decreased from 35° to 25°. Conversely, flue gas temperature exhibits nearly 20% reduction as swirl vane angle increased from 35° to 90°. Wang et al. [26] considered swirl vane angle of 35°, 45° and 55° in a down-fired boiler. It was demonstrated that maximum flue gas temperature for vane angle 35° was higher than vane angle 42° by approximately 43%. Increasing the vane angle from 42° to 53°, however, elevated the maximum flue gas temperature by nearly 100 °C. Sung and Choi [27] reported that high swirl (θ = 80°) operation reduces flame temperature considerably, owing to the more uniformly distributed coal particles that dissipated heat more effectively. Furthermore, it was also shown that radial turbulence intensity for θ = 80° operation is higher than that of θ = 40° operation by a factor of approximately 1.7. Overall, present findings on the effect of vane angle contradict each other. Bazooyar et al. [23,24] opined that a moderate vane angle of 45° would yield cleaner combustion than low (θ = 30°) and high (θ = 60°) swirl angles. Such findings concur with Wang et al. [26] as well. Nonetheless, the findings reported by González-Cencerrado et al. [28] are not aligned to such findings. They showed that a high vane angle promotes fuel-air mixing and lowers the NO_x emission instead of increasing it. Such dissent findings signify that detailed studies are still needed to examine the effect of vane angle on swirl combustion.

Despite several studies being conducted for dual fuel compression ignited (CI) engines [29,30], studies on biodiesel/NG dual fuel combustion in continuous swirl flame modes for gas

turbine are still scarce. Owing to the different operating principles between CI engines and gas turbines, dual fuel combustion characteristics acquired from internal combustion engines may not be suitably inferred to gas turbine burners, whereas the latter employs continuous swirl flames that comprises other complex coherent structures [18,31]. These flow structures have strong influence on energy exchange with the reacting shear layer [31,32]. Considering limited understanding on swirler vane angle and NG effects on biodiesel combustion in gas turbine, the present study intends to examine such effects using a model gas turbine swirl flame burner. Flame physical appearance, global combustion intermediate species and post-combustion emissions are characterised and empirical models are proposed for estimating post-combustion emissions of biodiesel/NG swirl flame.

2.0 Experimental Setup

In the present study, a reacting swirl flame was established using a model gas turbine swirl burner. Figure 1a illustrates the schematic diagram for the reacting spray rig used for the current study. Liquid fuel was delivered to the atomiser using a peristaltic pump (Longer BQ50-1J), equipped with a silicon tube of 4 mm inner diameter. A cylindrical chamber was utilised in order to remove the ripples generated via peristaltic motion prior to entering the atomiser. Finally, a twin-fluid air-blast atomiser (Delavan: SN type-30610-1) was used to atomise the supplied liquid fuel at an air-to-liquid ratio (ALR) = 2.5. Liquid fuel atomisation was achieved by introducing the desired amount of atomising air. As depicted in Fig. 1a, the supplied liquid fuel and atomising air were channeled to the atomiser through independent channels.

The swirl flame was then accomplished by the introduction of main air as shown in Fig. 1a. An axial swirler that consists of six straight vanes was placed concentrically at the burner outlet to generate swirl. Vane angles (θ) of 30°, 45° and 60° were examined, generating low, medium and high swirl, respectively. The swirler dimensions are depicted in Fig. 1b. The swirl number was calculated based on the equation 1 [33], where D_h, D_s and θ are the swirler hub diameter, swirler diameter and vane angle, respectively. Calculated swirl number for θ = 30°, 45° and 60° are 0.56, 0.84 and 1.12 respectively.

$$S_N = \frac{2}{3}\left[\frac{1-(D_h/D_s)^3}{1-(D_h/D_s)^2}\right]\tan\theta \qquad (1)$$

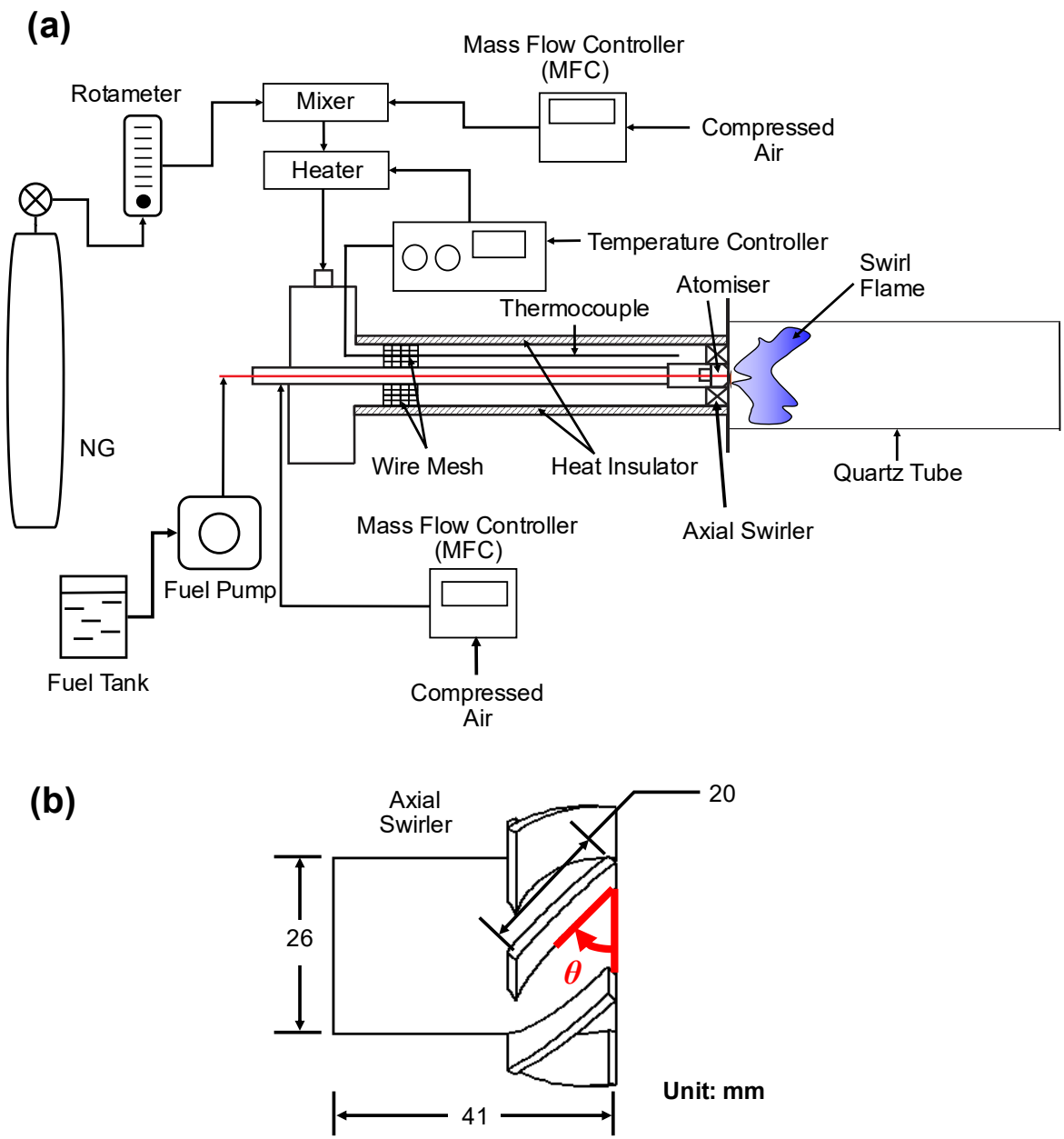

Fig. 1 (a) Schematic diagram for reacting spray rig, (b) Dimensions of axial swirler.

Wire meshes were employed to straighten the flow before the plenum exit. The main air was preheated using three rope heaters (Omega: FGR-100–240V, 500 W/rope) up to 250 °C. A 1.5 mm K-type thermocouple was positioned at 10 mm upstream of the burner outlet to acquire air temperatures. The thermocouple reading was feedback to a Proportional-Integral-Derivative

(PID) controller to effectively regulate the main air. To minimise the amount of heat losses, the plenum was also insulated with a 2 m long ceramic wool, as depicted in Fig. 1a.

For the reacting spray burner, the atomising process and the supplied air were regulated using Sierra SmartTrak 50 mass flow controllers (accuracy: ±1.5% full scale). Post-combustion products were channeled to the exhaust suction fan via a hollow carbon steel tube with 130 mm inner diameter and 400 mm long, as shown in Fig. 1a. For dual fuel operation, NG was fed from a high pressurised tank with the flow rate regulated using a rotameter, Fig. 1a. NG was premixed with the supplied main air in a gas mixer to form a homogeneous mixture prior to entering the burner plenum.

2.1 Fuels Tested

The fuels tested in this study include fossil diesel, palm biodiesel/methyl esters (PME) and NG. Fossil diesel was purchased from a local petrol station while PME was produced via transesterification from palm cooking oil. The cooking oil was heated up to 60 °C before being mixed with methanol and potassium hydroxide (KOH) blends. The ratio of lipid:methanol:KOH was fixed at 114:50:1 by mass. The mixture was then stirred for 3 hours using a magnetic stirrer at a constant temperature of 60 °C. The blended mixture was then collected to allow biodiesel and glycerol to separated. A decanting process was carried out to remove the produced glycerol. Then, the produced biodiesel was heated up to 120 °C in order to remove the remaining water and methanol contents. This evaporation process was conducted for approximately 4 hours.

In characterising the produced biodiesel, a gas chromatography (Agilent 7820A) was used to determine the yield of the biodiesel based on EN 14103 standards. Major fatty acids composition

for all biodiesels produced are provided in Table 1. It is noticeable that PME is a mixture of unsaturated (Oleic and Linoleic) and saturated (Palmitic and Stearic) fatty acids. Besides this, PME is also shown to consist of pre-dominantly longer fatty acid chains (C16 and C18), which resulted in a higher average molecular weight than diesel. Degree of unsaturation (DOU) and mass average chain length (CL) for the PME were determined as 0.62 and 17.2, respectively, based on equations 2 and 3 [34]. The parameter *C* represents the numbers of carbons in the fatty acid *i*, with the term *n* representing mass proportions of the latter. The term *B* represents the number of double bonds. Several important physical properties that are frequently being reported in combustion literatures are delineated in Table 2.

Table 1 Percentage of fatty acids composition by mass in PME.

Fatty Acid	**No of carbon: double bond**	**Composition (% wt)**
Caprylic	(C8:0)	0.8
Capric	(C10:0)	-
Lauric	(C12:0)	-
Myristic	(C14:0)	1.1
Palmitic	(C16:0)	42.5
Stearic	(C18:0)	4.2
Oleic	(C18:1)	41.3
Linoleic	(C18:2)	9.5
Linolenic	(C18:3)	-
Others		0.6

Table 2 Physical properties for diesel and PME.

Properties	**Unit**	**Diesel**	**PME**
Lower heating value* (LHV)	[MJ/kg]	42.6	37.4
Density*	[kg/m^3]	843.3	867.7
Cetane number** (CN)	[-]	52.0	62.0
Flash point**	[°C]	72.0	163.0
Kinematic viscosity** (40°C)	[mm^2/s]	2.6	4.6
Pour Point**	[°C]	-20.0	5.0
Molecular weight† (MW)	[g/mol]	226.0	270.1
Stoichiometric air fuel ratio† (AFR_s)	[-]	14.8	12.3

* Measured

** Taken from [7,33]

† Calculated

$$CL = \frac{\sum_{i=1}^{n}(n_i C_i)}{100} \tag{2}$$

$$DOU = \frac{\sum_{i=1}^{n}(n_i B_i)}{100} \tag{3}$$

The Natural Gas used was purchased from Gas Malaysia Berhad (GMB) through a local industrial gas supplier. NG compositions and physical properties are listed in Table 3 [35].

Table 3 Typical component and physical properties of NG [35].

Component	Typical range (Mole %)	Properties	Unit	
Methane	84.04	LHV	[kCal/m^3]	8,862
Ethane	4.95	Specific Gravity	[-]	0.68
Propane	1.62	Burning Velocity	[m/s]	0.28
Isobutane	0.12	Autoignition Temperature	[°C]	537
n-Butane	0.07			
Isopentane	0.07	AFR_S	[-]	17.3
n-Pentane	0.03			
Hexane	0.03			
Nitrogen (N_2)	1.59			
CO_2	7.48			

2.2 Operating Conditions

Diesel and neat PME were chosen as baseline fuels in the present combustion study. PME/NG dual fuel combustion was tested at three different input power proportions, namely P90N10, P80N20 and P70N30. The ratio 90 indicates that 90% of the input power comes from the PME, while the remaining 10% is supplied by the NG, as described by equation 4. $\dot{m}_{PME}$ and $\dot{V}_{NG}$ represent mass flow rate and volume flow rate, respectively. As such, mass flow rate for PME in the P90N10 combustion would be lower than neat PME. For P80N20 and P70N30, the flow rate for PME was reduced further, whereas the mass flow rate of NG was increased to compensate for the reduction of PME input thermal power. All flames were established under constant thermal input power ~9.3 kW.

$$\dot{m}_{PME} LHV_{PME} : \dot{V}_{NG} LHV_{NG} = 90:10 \quad (4)$$

2.3 Measurement techniques

Global flame images were captured using a digital camera (Canon EOS 600D) through a transparent quartz tube. Flame spectrums were captured using a spectrometer (Ocean Optics, Maya2000Pro). The operating range of spectrometer spans from wavelengths 200–600 nm. KANE Quintox 905 gas analyser was utilised to quantify post combustion products (NO, CO and CO_2) at the combustor outlet. CO and NO were measured using chemical sensors, whereas CO_2 was calculated from oxygen (O_2) measurements. The NO and CO emissions reading were subsequently corrected to 16% O_2 for gas turbine operation [36]. The sampling probe of the gas analyser has an inner diameter of 5 mm with a sampling rate of 2 L/min. Calibration gases were used to cross check the analyser prior to measurements. The sampling probe was placed at a distance of 13 mm inward from the combustor outlet to avoid ambient air dilution. The sampling was taken at five spatial positions that are evenly spaced radially across the combustor outlet. The probe is set to take samples for 2 minutes at each spatial location to ensure a steady state reading. An area-velocity weighted averaging method was then used to obtain global average specific emissions for each test case. Every measurement is associated with uncertainties that affect their final answer. The propagated error method was used to quantify uncertainties associated with the measurements of this study. The measurement range, uncertainty and propagated errors of the gas analyser and spectrometer are shown in Table 4.

Table 4 Specifications of gas analyser and spectrometer.

Sensor/ Instrument	**Range**	**Resolution**	**Uncertainty**	**Propagated Error**
NO	0-5000 ppm	1 ppm	<100 ppm; ± 5 ppm >100 ppm; ± 5%	± 7.5%
CO	0-4000 ppm	1 ppm	<100 ppm; ± 5 ppm >100 ppm; ± 5%	± 16.0%
O_2	0-30%	0.01%	± 0.2%	± 1.3%
Spectrometer	200-1000 nm	0.1 nm	± 0.1 nm	± 1.3%

3.0 Results and Discussion

3.1 Flame Visualisation

Figure 2 compares swirl flame shapes of diesel, PME and PME/NG for θ = 30°, 45° and 60°, at global flame equivalence ratio 0.65. The physical appearance of diesel swirl flames evolves remarkably as vane angle increases from 30° to 60°. The luminosity increases in the orange-yellowish flame brush downstream of the main diesel reaction zone, contracting significantly as vane angle increases from 30° to 45°. The sooty flame brush is practically vanished as vane angle increases further from 45° to 60°. This is attributable to the highly energetic swirling flow at θ = 60° that accelerates soot particles oxidation, leaving only insignificant amounts of soot particles downstream the diesel main reaction zone.

PME and PME/NG flames showed no distinct variation in their colour as vane angle increases from 30° to 60°, whereas swirling flames for both types of fuels remain bluish in colour. Nonetheless, the luminous main reaction area for θ = 30° is notably larger than that of θ = 60°. This is primarily due to the weakened swirling force in θ = 30° operation that hinders reactants radial diffusivity. This, along with inadequate air entrainment into the dense spray core slow down the soot particles oxidation rate. For θ = 60° operation, enhanced radial dispersion force promotes fuel-air mixing that subsequently accelerates the reaction rate, resulting in considerably smaller luminous reaction zone than θ = 30° operation. For biodiesel, however, changing in the size of reaction zones is less significant when vane angle varied from 30° to 60°. This is presumably due to the higher biodiesel molecular weight and lower volatility that reduce its susceptibility against the variation in radial dispersion force.

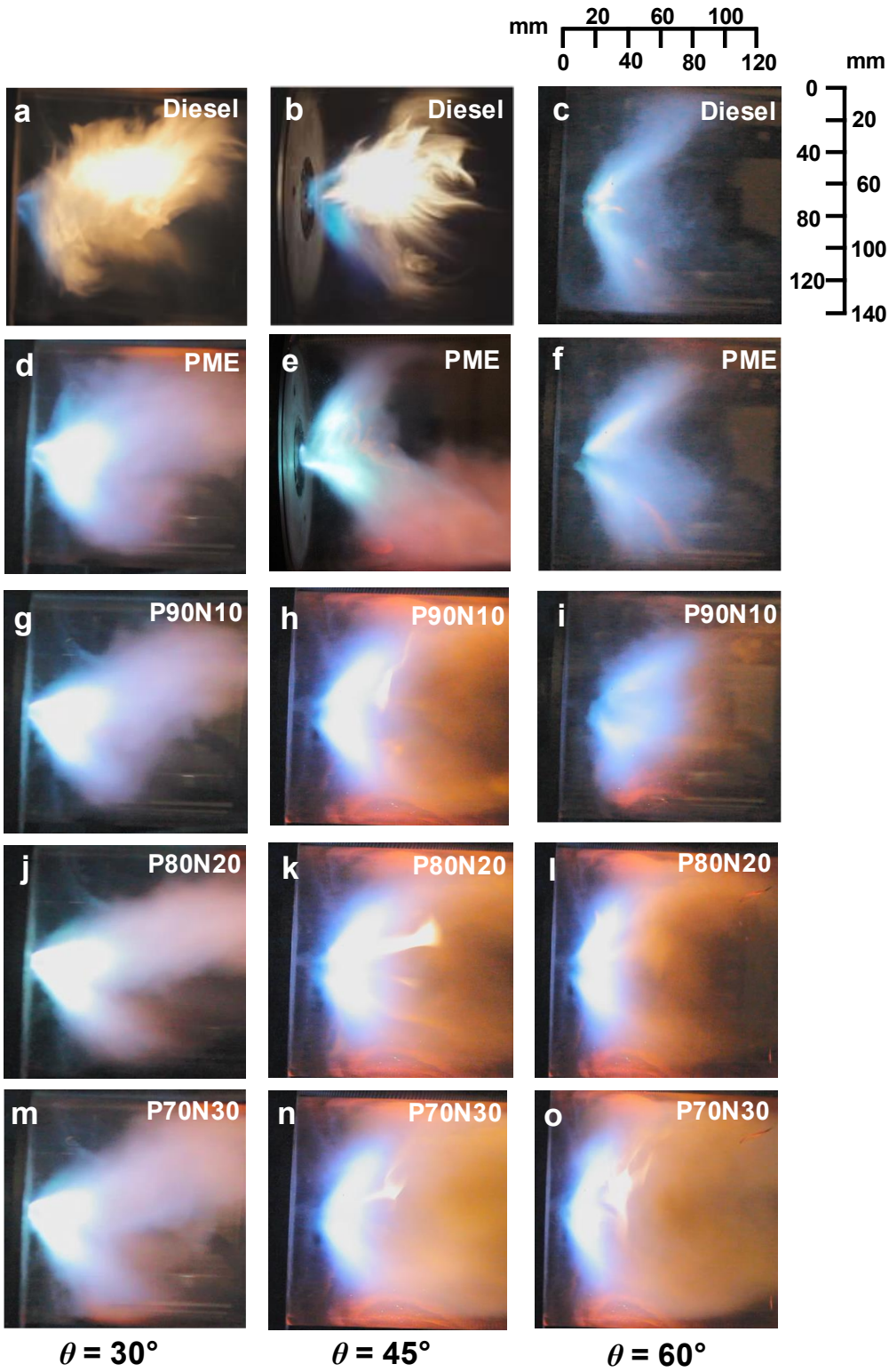

Fig. 2 Images for diesel, PME and PME/NG swirl flames established at θ = 30°, 45° and 60°, φ = 0.65, ALR 2.50 and main air temperature 250 °C.

The PME/NG swirl flame exhibits a subtle liftoff from the base of the burner for θ = 45° and 60° operations. Nonetheless, the slight detachment of PME/NG swirl flame from the burner base does not affect overall stability of the flame. Such liftoff is presumably due to the high specific heat of the NG (approximately two times higher than air at 1500 K and constant pressure [37]), whereas NG has absorbed a portion of the heat needed for ignition at the burner outlet, thus shifting the ignition and stabilisation of flame to a slightly downstream position. Close observations were reported by [38,39], where it was demonstrated that addition of NG to the liquid spray flame incurs segregation of OH^* chemiluminescence signal at immediate burner outlet, signifying that local extinction takes place at near burner outlet. However, flame liftoff does not happen to the θ = 30° operation. Weakened vortical flow in θ = 30° operation decelerates droplet diffusivity and evaporation rate. This inherently promotes droplet group combustion that prone of elevating the flame temperature [18]. Such elevation in temperature would have offset the heat absorbed by NG.

3.2 Flame Spectroscopic Analysis

Figure 3a compares flame spectra for P70N30 for θ = 60°, 45° and 30°, while Fig. 3b compares flame spectra of PME, P90N10, P80N20 and P70N30 for θ = 60°. Figure 3a shows that OH^* (Hydroxyl), CH^* (Carbyne), C_2^* (Diatomic Carbon) and CN^* (Cyanido) intensities for θ = 30° is higher than for θ = 60°. P70N30, on the other hand, produces the highest spectral intensities in Fig. 3b.

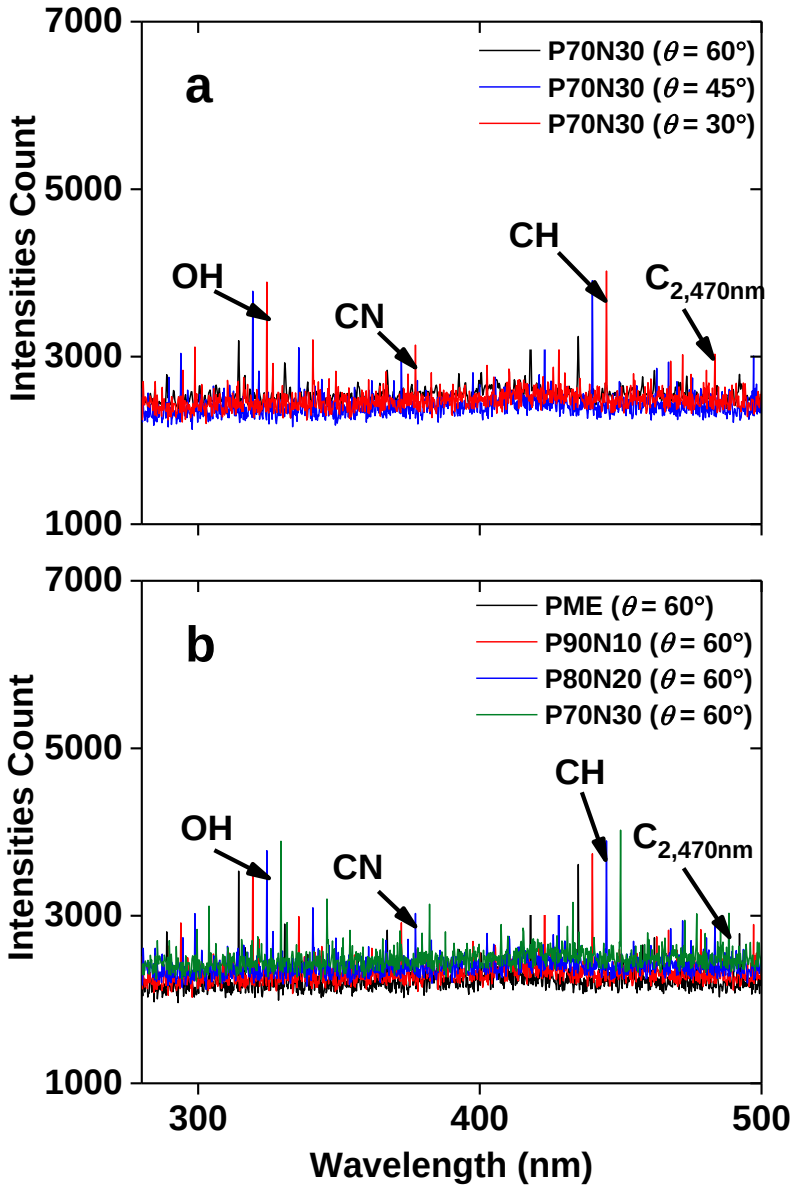

Fig. 3 Flame spectra for (a) P70N30 at three different vane angles and (b) PME and PME/NG at θ = 60°, φ = 0.65, ALR 2.5, main air temperature 250 °C.

Figure 4 unveils that OH^* and CH^* intensities at φ = 0.65 are higher than at φ = 0.9 by a factor of ~1.05. This is mainly due to the increased air supply at φ = 0.65 that strengthens the vortical core of the swirling flow. Higher turbulent energy dissipation rate at φ = 0.65 leads to a more vigorous fuel/air blending, shortening the reaction time scale and gives rise to the radical production. It was shown previously that OH^* intensity exhibits a positive correlation with reduced fuel/air mixing time scale [40]. Moreover, increased O_2 supply at lower equivalence ratio comprises another plausible reason for the higher OH^* intensity.

It is shown in Fig. 4 that θ = 30° elevates OH^* and CH^* intensities by averaging 1.2 times as compared to θ = 45° and 60. Such increment can be attributed to the weakened vortical flow at θ = 30° operation that decelerates radical consumption rate within the reaction zone. In contrary, OH^* and CH^* intensities for θ = 60° operation are noticeably lower than that of θ = 45°and 30°. Strengthened vortical flow promotes radical consumption rate, resulting in a less intense reaction zone. Moreover, higher scalar dissipation rate due to the highly turbulent flow at θ = 60° comprises another plausible reason for the lower OH^* and CH^* intensities. Transport of radicals out of the flamelet is expected to be faster than production rate in the flamelet, resulting in less radicals produced. It was observed that OH^* mole fraction is reduced by nearly half as scalar dissipation rate increased by an order of magnitude [40].

Meanwhile, it can be observed also from Fig. 4 that OH^* and CH^* intensities are increased as higher NG mass fraction is introduced. Spectra intensities are elevated by a factor of averaging 1.4 when the fraction of NG input thermal energy increased from 0% to 30%. This denotes that NG addition intensifies the overall reaction rate. Such escalation in reaction rate can be attributed to NG is mainly composed of methane. Chain length for methane is significantly shorter than that of biodiesel, leading to accelerated decomposition rate that intensifies the reaction. An intensified

reaction rate subsequently delivers more energy by fuel decomposition processes, leading to high H^* radical and short alkyl radical (such as CH_2^*) concentrations that are essential to produce OH^* and CH^* radicals [41–44].

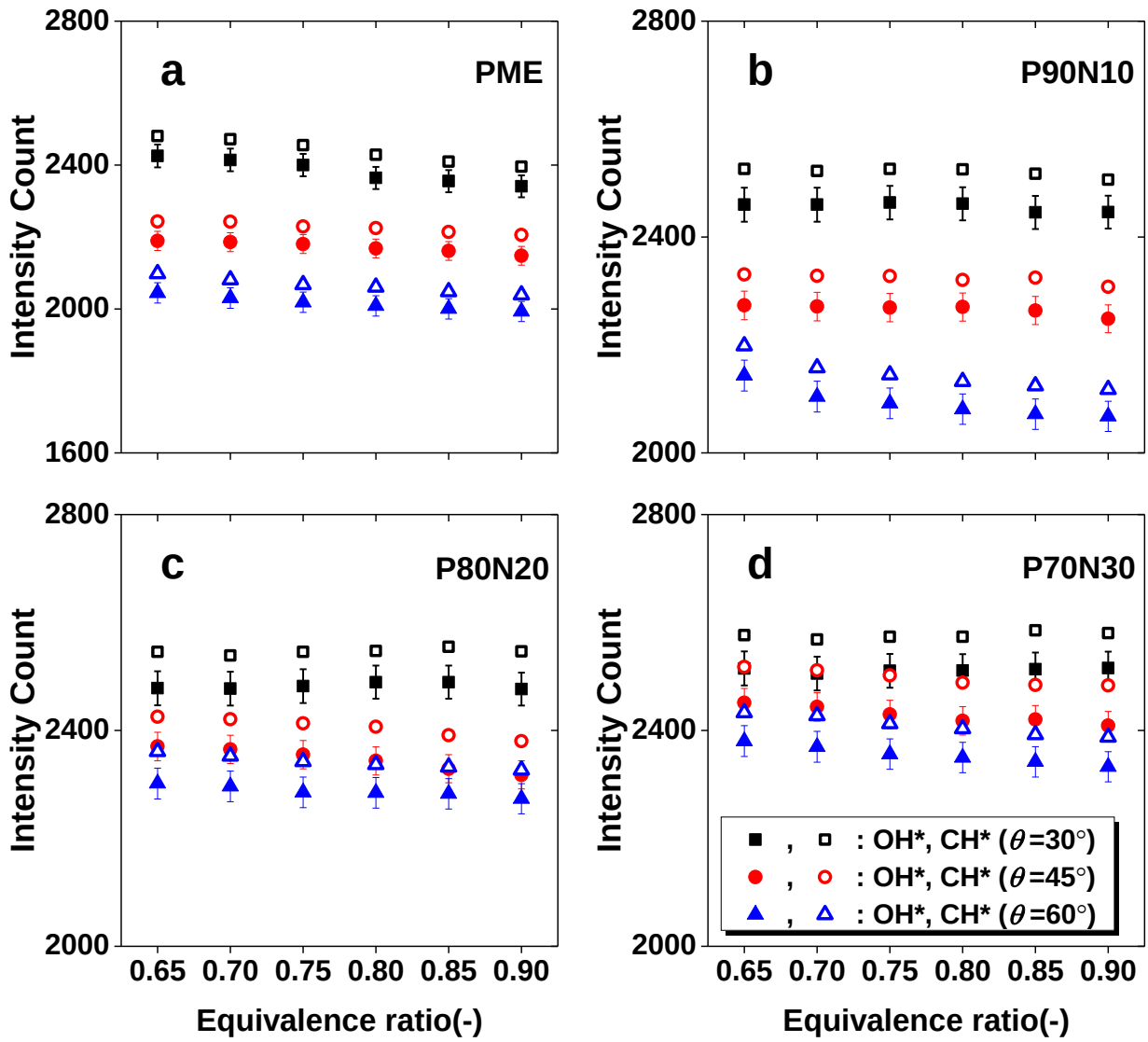

Fig. 4 Intensities count of OH^* and CH^* against equivalence ratio for (a) PME, and (b-d) PME/NG at ALR 2.5, main air temperature 250 °C.

Figure 5 compares intensities of CN^* and $C^*_{2,470nm}$ for neat PME and PME/NG from φ=0.65 to φ=0.9. Like OH^* and CH^*, intensities of CN^* and $C^*_{2,470nm}$ also exhibit a negative correlation with increased global flame equivalence ratio. This hints that the formation of CN^* and $C^*_{2,470nm}$ are correlated with OH^* and CH^*. This is because CH^* and H^* are primary species needed for CN^* and $C^*_{2,470nm}$ production [45]. Meanwhile, as shown in Fig. 5, NG addition also has notable effects on CN^* and $C^*_{2,470nm}$ production, mainly as a consequence of more OH^*, C^*, CH^*, HCN^* and CH_2^* produced in dual-fuel operations. CH^* and CH_2^* would tend to react with C^* or CH^* radical to form C_2^* radical [45] while CH^* would react with N_2 to form HCN* [46], thus elevating the concentrations of C^*_2 and CN^* radicals as illustrated in Fig. 5. The present research shows that increased NG input power fraction leads to intensified global reaction, as reflected by noticeably higher radical intensities for dual fuel combustion in Fig. 4 and 5. Even though PME/NG flames exhibit slight liftoff from the burners' base, the effects on overall flame stability are inconsequential in the present operating range. The intensified reaction in dual fuel combustion has neutralised flame instability provoked by local extinction at the burners' base.

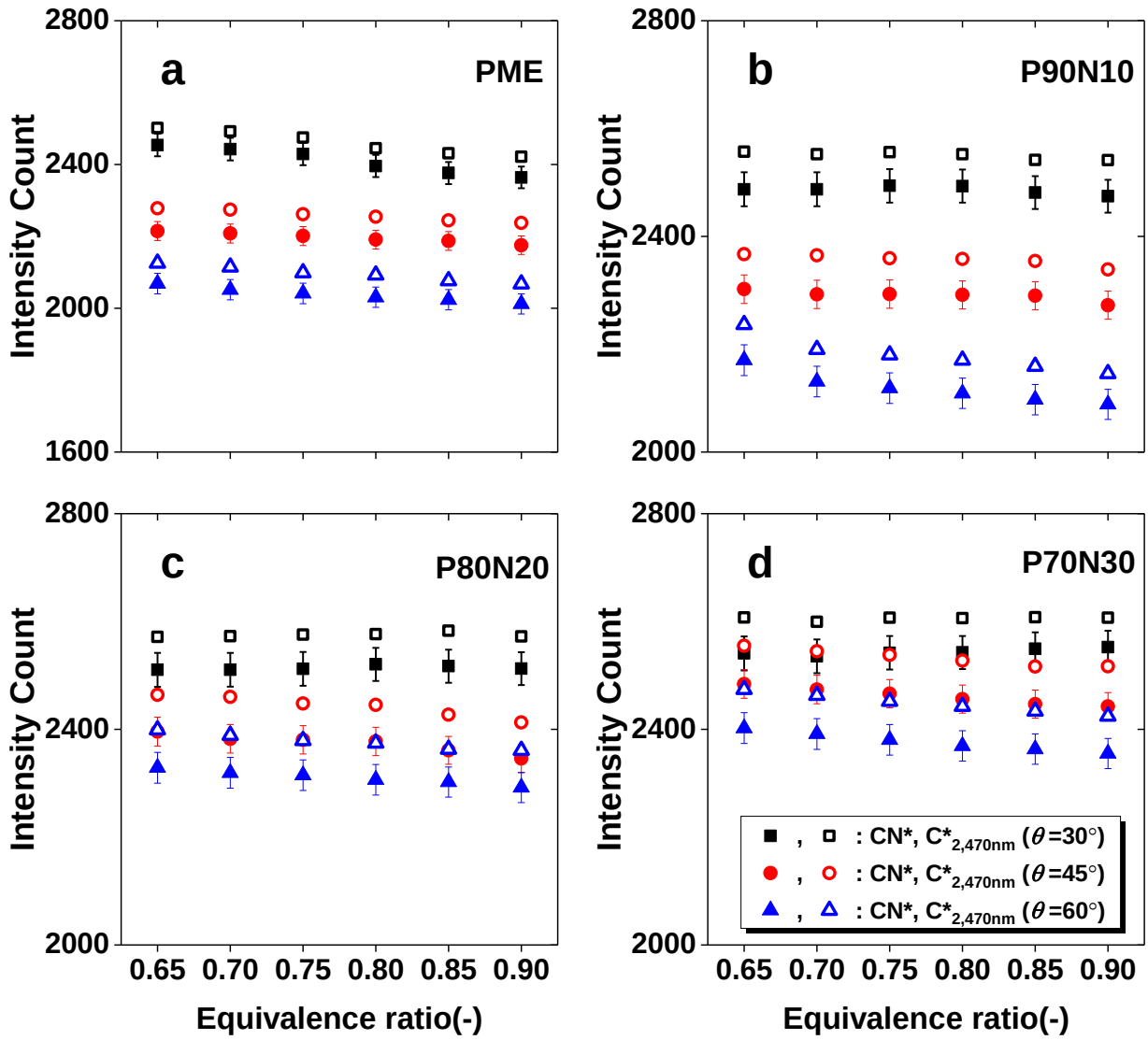

Fig. 5 Intensities count of CN^* and $C^*_{2,470nm}$ against equivalence ratio for (a) PME, and (b-d) PME/NG at ALR 2.5, main air temperature 250 °C.

3.3 Post Combustion Emissions

Figure 6 compares NO emissions of neat PME, and PME/NG flames for the three different vane angles. The effect of vane angle variation on NO production is pronounce. NO emissions of PME, and PME/NG increased by ~22% as the vane angle was reduced from 45° to 30°. On the contrary, NO emissions are reduced by nearly 86% as the vane angle is increased from 45° to 60°. For θ = 30° operation, lower turbulent kinetic energy provokes a larger turbulent length scale that undesirably lowers the turbulent energy dissipation rate. This provokes poor mixing between reactant and oxidiser. Less homogeneous fuels/air mixture leads to prolonged droplet evaporation and reaction time scales, giving rise to the local flame temperature. This is also reflected by the considerably high OH^* and CH^* intensities for θ = 30° operation in the earlier section. Increased reaction zone temperature subsequently promotes thermal NO formation. Conversely, for θ = 60° operation, higher turbulent kinetic energy reduces the turbulent length scale and accelerates turbulent energy dissipation rate. This enhances the mixing between PME, NG and air, forming a more homogeneous combustible mixture. Hastened reaction rates with vigorous air flows expedite heat production and heat transfer out of the flamelet, rendering less heat for thermal NO production. This is observed by the drastic NO emission reduction in 60° vane angle operation.

Figure 7 denotes that P70N30 combustion produces significantly lower NO emission than PME (up to a factor of averaging 3.5). The lowest NO emission from P70N30 flames are attributed to the increased NG mass fraction that shifts considerable portion of the non-premixed combustion into premixed mode. Premixed NG-air is a homogeneous combustible mixture that can react at much faster rates than PME droplets. This prevents the formation of local high temperature regions, suppressing thermal NO production as a consequent.

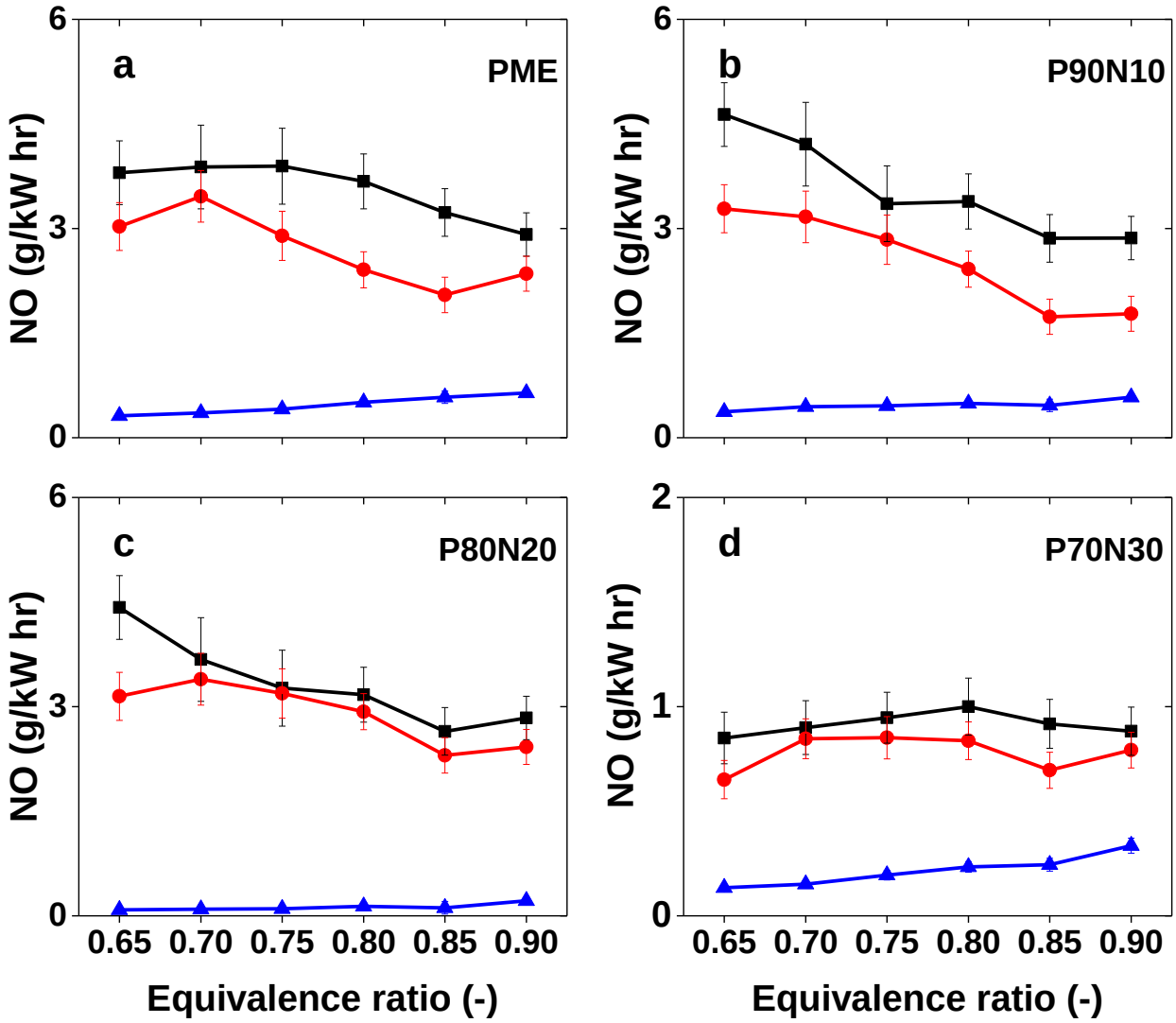

Fig. 6 NO emission against equivalence ratio for (a) PME, and (b-d) PME/NG at ALR 2.5, main air temperature 250 °C. (■ θ = 30°, ● θ = 45°, ▲ θ = 60°)

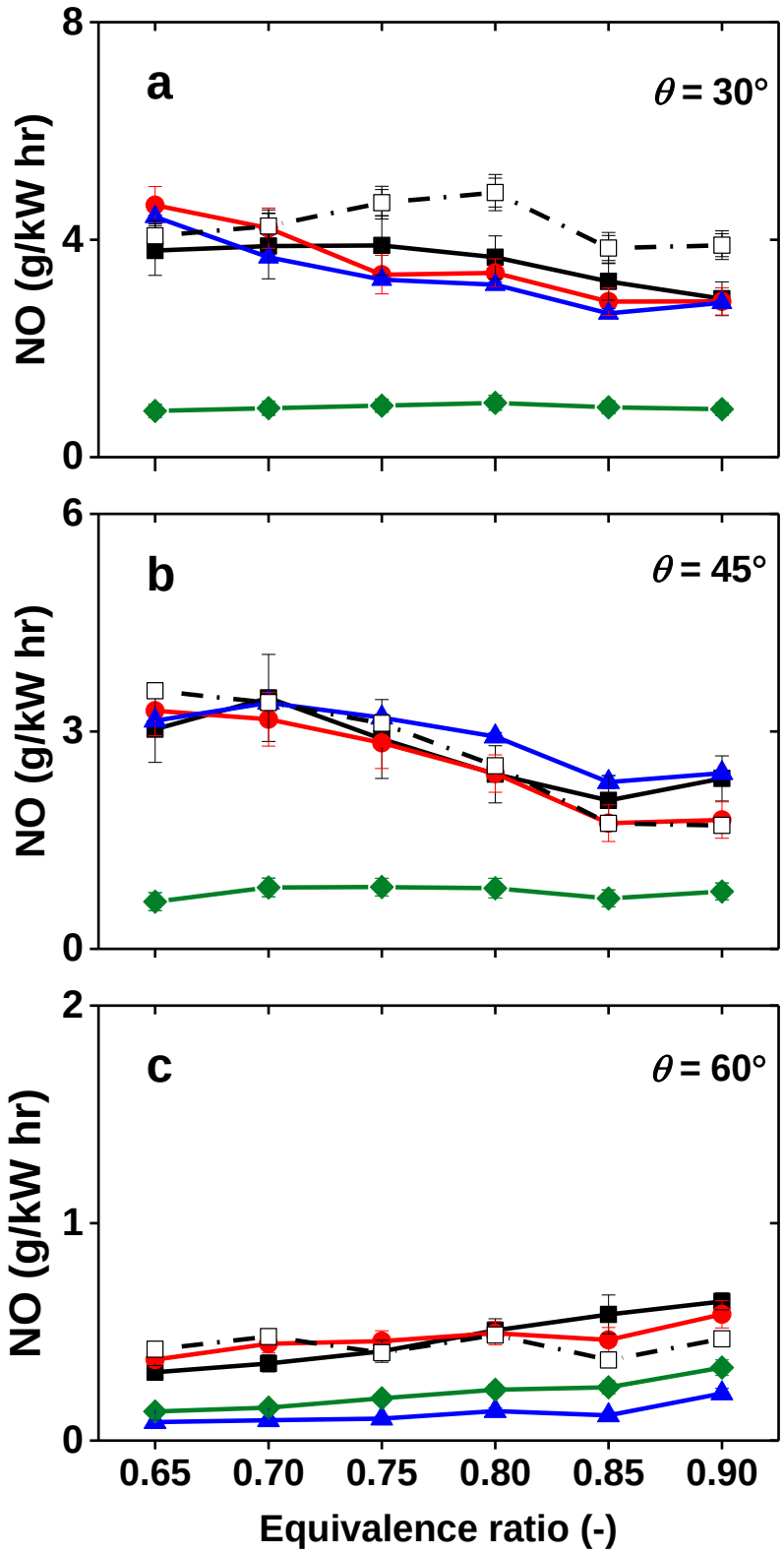

Fig. 7 PME and PME/NG's NO emission comparisons for vane angle (a) 30°, (b) 45° and (c) 60°, at ALR 2.5, main air temperature 250 °C. (■ PME, □ Diesel, ● P90N10, ▲ P80N20, ♦ P70N30)

Furthermore, due to the substantial reduction in PME flow rate and atomising air in P70N30, the PME fuel jet precession momentum is weakened thereupon. This enables swirling flow to displace significant portion of PME droplets radially outwards. The intensity of inner reaction zone is inherently lowered due to the decreased droplet number density, comprising another tenable explanation for the reduced local high temperature regions and thermal NO production in P70N30 combustion. Scattered reaction zones in dual fuel operation were also reported by Evans et al. [38], where dual peak temperatures were identified along the radial direction of n-Heptane/NG swirl flame. Thus, even though P70N30 combustion yields the highest global reaction intensities (for a given vane angle), shifting of combustion mode and the dispersions of reaction zones suppress local hot regions formation and thermal NO production. On the contrary, disparities in NO emission between neat PME, P90N10 and P80N20 are only marginal for θ = 30° and 45° operations, as seen in Fig. 7. This can be attributed to the relatively low NG mass fraction in these cases, where combustion mode remains pre-dominantly non-premixed. The present study unveils that NG input power fractions of 20% and 30% together with a swirler vane angle 60° are desirable for effective NO reduction in PME/NG combustion.

In addition to examining post-combustion emissions, the present research also proposes that correlation between specific NO emissions and vane angle for PME and PME/NG at φ = 0.65 can be approximated by linear correlation delineated by equation 5. The global equivalence ratio 0.65 was chosen for establishing the empirical correlation since gas turbine typically operates in the fuel-lean regime. Empirical models for estimating the gradient (m) and y-interception (c) in equation 5 are proposed in Fig. 8, where both coefficients are of quadratic functions of NG input power fractions.

$$NO = (m\theta) + c \tag{5}$$

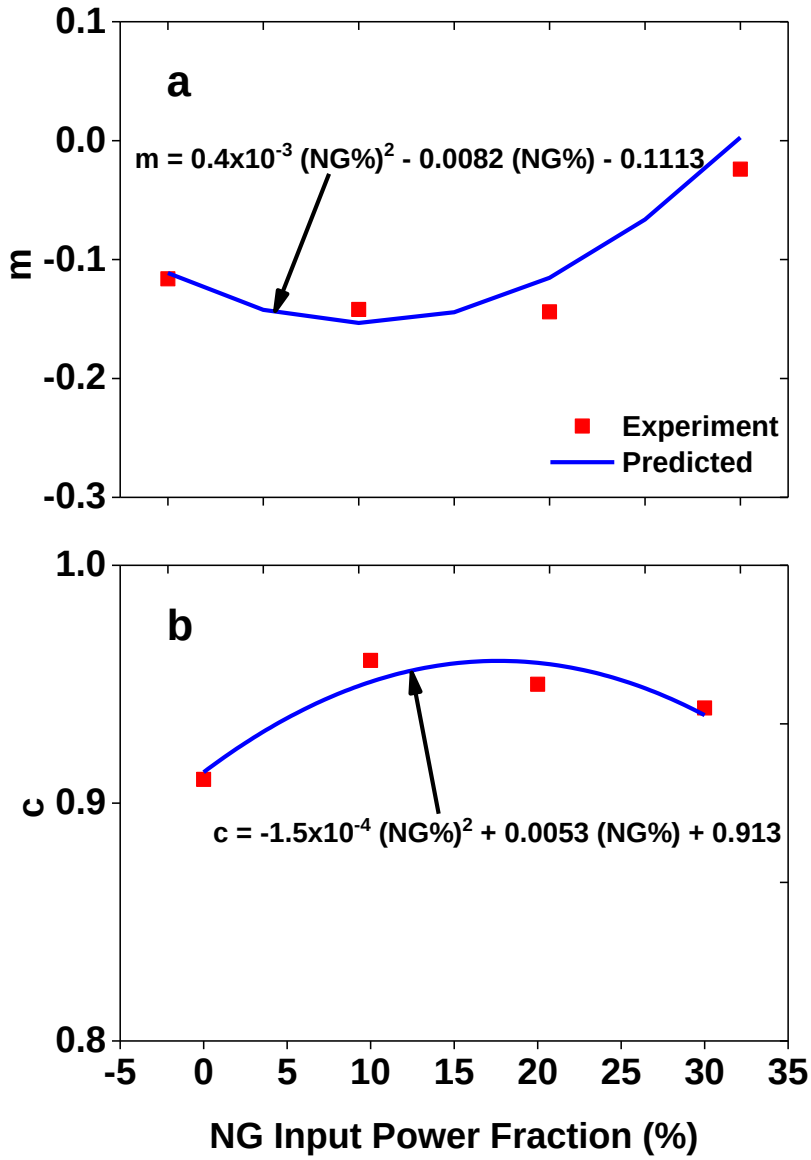

Fig. 8 (a) *m* and (b) *c* correlation with NG input power proportion for equation 5.

Figure 9 shows the outcome of NO estimation based on equation 5 and Fig. 8. It is evident from Fig. 9 that the proposed empirical models can estimate specific NO emission of PME and PME/NG combustion for different vane angles satisfactorily at φ = 0.65. R^2 for the estimation

curves are considerably high as shown in Fig. 9, indicating that the proposed models are reliable tools for predicting NO emission from PME and PME/NG combustion in the specified operating range and conditions. Overall, estimation curves in Fig. 9 shows that NO emission is lowered as vane angle increased from 30° to 60°. Such estimation concurs with previous study by Cencerrado et al. [28].

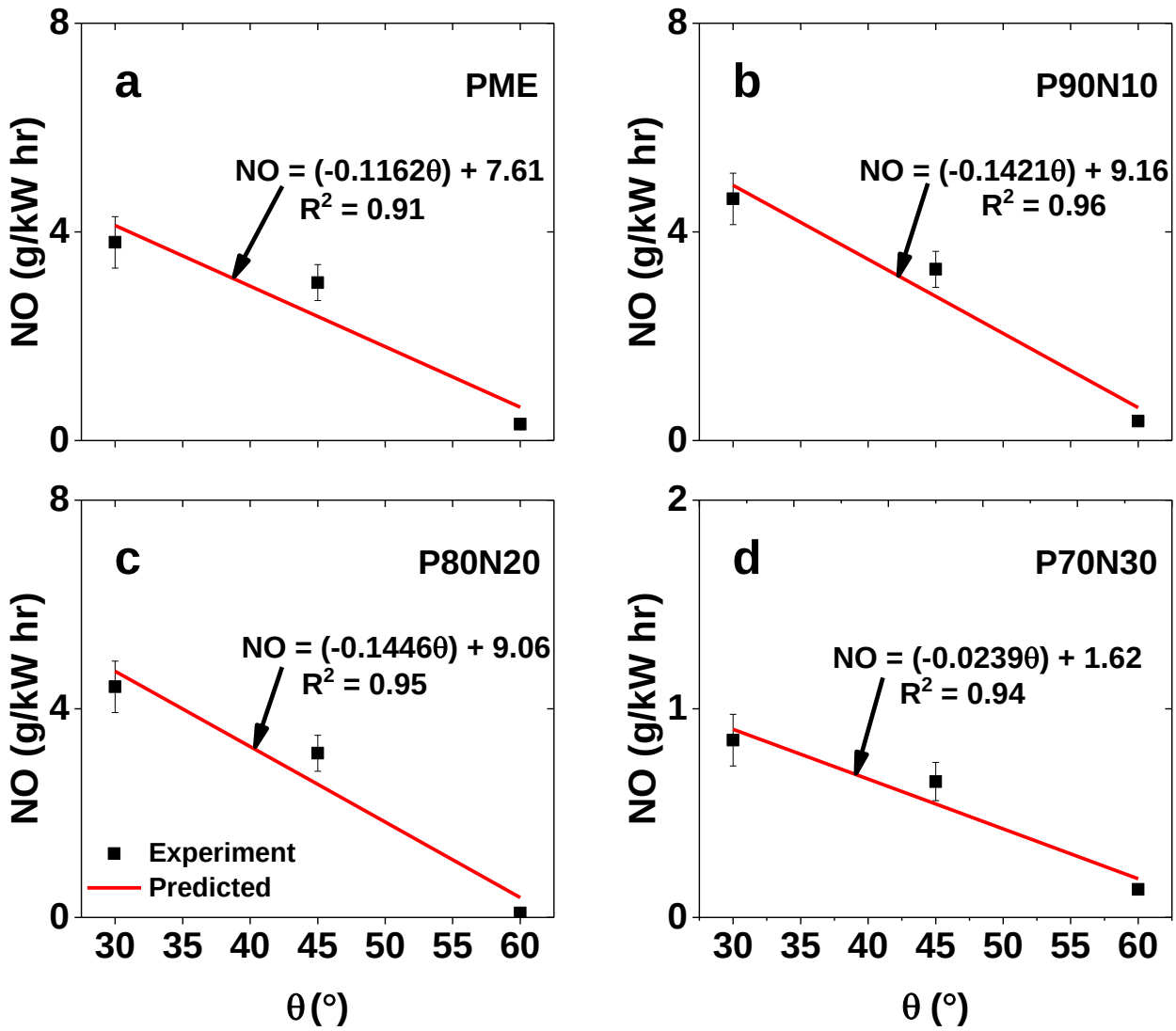

Fig. 9 NO emission prediction for (a) PME and (b-d) PME/NG against different vane angles at φ = 0.65, ALR 2.5, main air temperature 250 °C.

The effect of vane angle on CO emission for PME and PME/NG is shown in Fig. 10. It is shown that high vane angle operation does not guarantee CO reduction. Although θ = 60° shows generally lower CO than θ = 30° and 45°, but disparities in CO emission between different vane angles are not significant. High swirl operation is expected to prompt the formation of small-scale turbulent eddies that enhance CO-oxidiser blending, converting most of the CO into CO_2. However, the trend in Fig. 10 shows incongruity, denoting that heat transfer out of the flamelet in θ = 60° operation is pronounced, leaving lesser amount of heat that is essential for CO to CO_2 oxidation.

Although P70N30 shows promising NO emission improvement against neat PME, its improvement for CO emissions against neat PME is not significant, as shown in Fig. 11. NG addition promotes intense combustion and carbon reduction, and this is expected to lower the CO emission correspondingly. The observed comparable CO emission between dual fuel operating mode and neat PME is presumably due to the reduction in atomising air stream velocity in the dual fuel operating mode (due to the reduction in PME fuel flow rate). This weakens the interaction between liquid and air streams, hindering liquid disintegration processes consequently. Nonetheless, such deterioration in atomisation quality is offset by NG addition and this leads to comparable CO emissions with neat PME. Meanwhile, another plausible reason would be that methane combustion has consumed a portion of the O_2, leaving the biodiesel to burn in relatively fuel-rich condition that gives rise to the CO emission. In general, CO emission from diesel, PME and PME/NG flames are rather low, whereas disparities between one another are only marginal. Extreme low CO emission in biofuel swirl flames were also reported by [36], implying that swirl combustion is an effective way of minimising CO emissions.

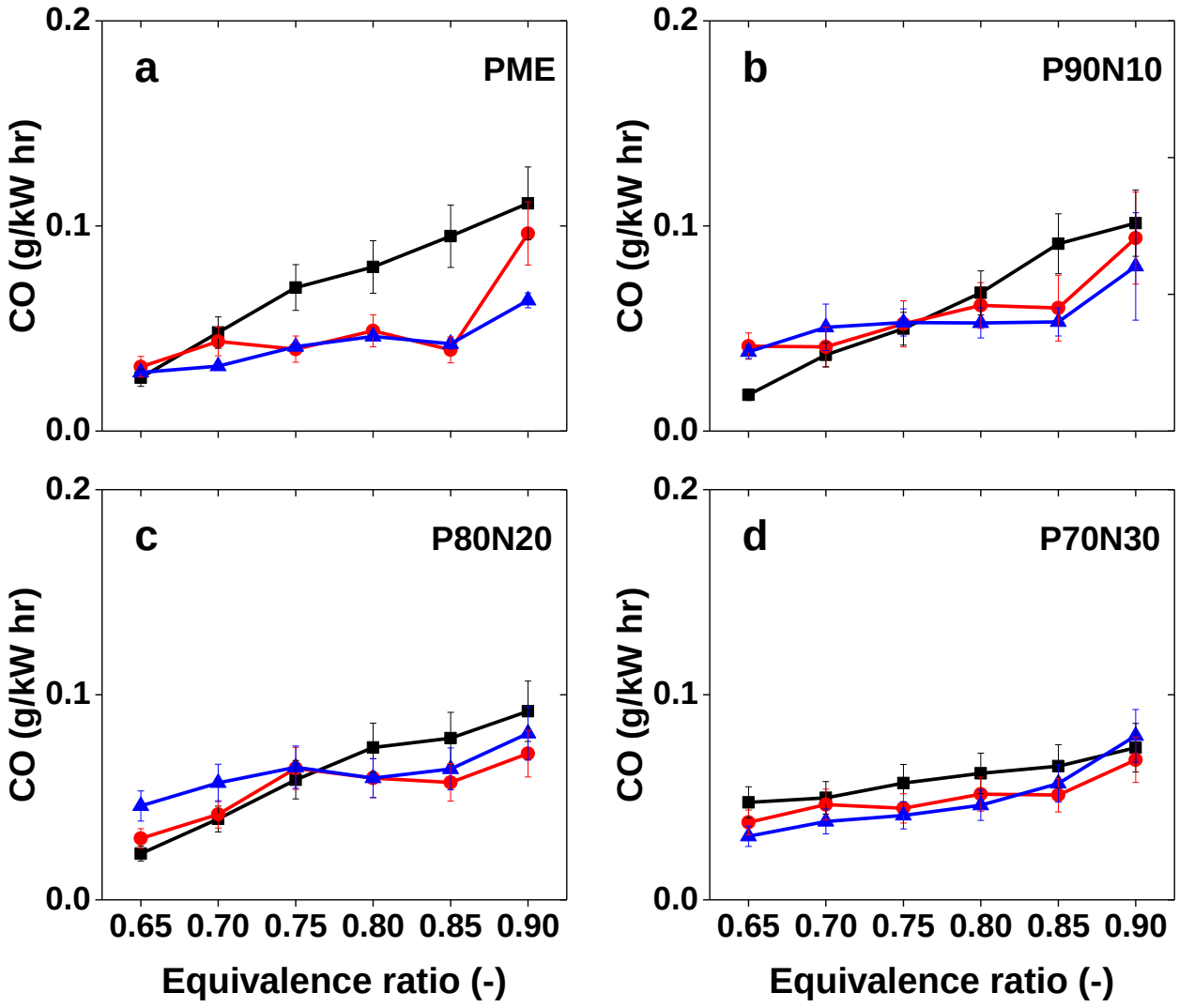

Fig. 10 CO emission against equivalence ratio for (a) PME, and (b-d) PME/NG at ALR 2.5, main air temperature 250 °C. (■ θ = 30°, ● θ = 45°, ▲ θ = 60°)

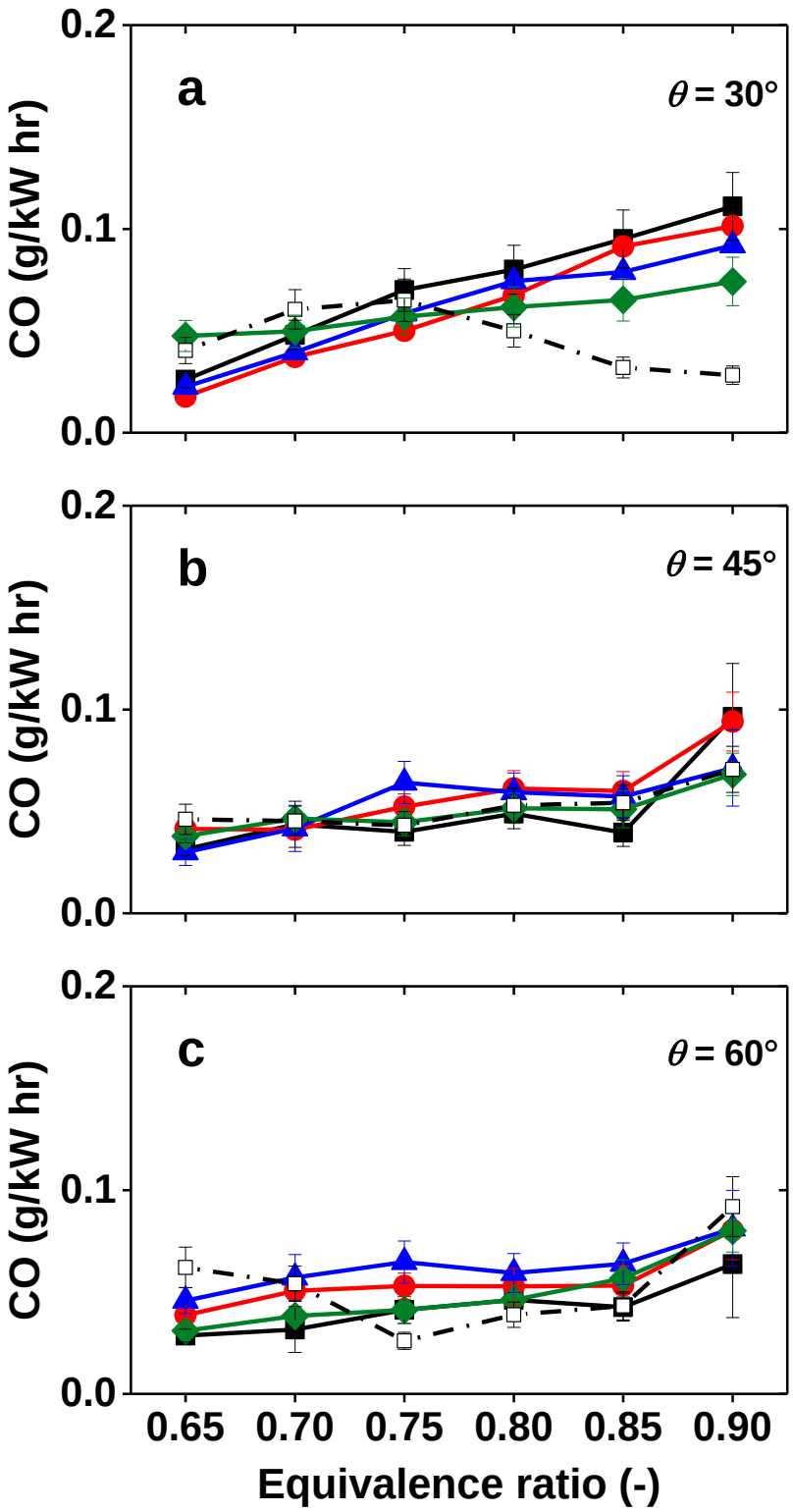

Fig. 11 PME and PME/NG's CO emission comparisons for vane angle (a) 30°, (b) 45° and (c) 60°, at ALR 2.5, main air temperature 250 °C. (■ PME, □ Diesel, ● P90N10, ▲ P80N20, ◆ P70N30)

4.0 Conclusions

The present research examines PME, PME/NG and diesel combustion characteristics employing different geometries with vane angles of θ = 30°, 45° and 60° for different swirl numbers at a constant input thermal power of 9.3 kW. The PME/NG swirl flame is mainly characterised by a slight flame liftoff. High vane angle of 60° strengthens the vortical flow, directing the flame towards radial direction while inhibiting axial flame propagation. This results in a thinner luminous reaction zone as compared to those of θ = 45° and 30°. Meanwhile, OH^*, CH^*, CN^* and C_2^* intensities for PME/NG are higher than that of neat PME, owing to the presence of ethane in the NG that intensifies the reaction. Flame instability provoked by liftoff is offset by the intensified reaction in the present operating range. Moreover, high dissipation rates at θ = 60° operation lead to noticeably lower radical intensities as compared to θ = 45° and 30° combustion.

Emission wise, P70N30 combustion produces NO emissions that are lower than neat PME and diesel. This is partly due to considerable portion of the combustion mode has been replaced by premixed NG combustion. On top of this, NO emissions for PME and PME/NG combustion are reduced significantly when operating with vane angles of θ = 60°, owing to the substantial reduction in thermal NO. The differences in CO emission between PME/NG, PME and diesel are not significant. Nonetheless, vigorous flows at θ = 60° expedite CO oxidation, producing remarkably low CO emission. The present study also proposes empirical models for estimating NO emission from PME and PME/NG combustion at different vane angles. For any given NG and PME input power fractions, NO emission at φ = 0.65 can be obtained without the need to perform measurements. Overall, the present study shows that NO emissions for the dual fuel operation can be optimised by varying NG input power fractions to over 20%, along with φ = 0.65 and a swirler vane angle of 60°. The PME/NG co-firing has shown to be a feasible alternative fuel for land-

based gas turbines because it is found to be cleaner than neat PME and diesel, while maintaining comparable flame stability against baselines in a model gas turbine combustor. These works set a promising path for the development of units capable of co-firing multi-phase fuels to address the challenges of NO emissions and unwanted instability issues in flexible gas turbines.

Acknowledgement

Meng-Choung Chiong thanks the financial support from Universiti Teknologi Malaysia through Vot Amanah Makmal Aeronautik (A.J510600.5549.07134) and Ministry of Higher Education Malaysia through MyBrain sponsorship. **Agustin Valera-Medina** gratefully acknowledges the support from the Welsh European Funding Office (WEFO) through its program "Flexible Integrated Energy Systems (FLEXIS)", project no. 80835. **Cheng Tung Chong** acknowledges the funding support from The Royal Society, Malaysian Industry-Government Group for High Technology and The Academy of Sciences Malaysia under the Newton-Ungku Omar Fund: Advanced Fellowship (NA160115).

CRediT authorship contribution statement

Meng-Choung Chiong: Conceptualization, Methodology, Investigation, Validation, Formal Analysis, Visualization, Writing - original draft, Writing - review & editing. **Agustin Valera-Medina:** Writing - review & editing. **William Woei Fong Chong:** Project administration, Methodology, Funding acquisition, Writing - review & editing. **Cheng Tung Chong:** Writing -

review & editing, Resources. **Guo Ren Mong:** Investigation, Data Curation. **Mohammad Nazri Mohd Jaafar:** Project administration, Resources.

Declaration of Competing Interest

The authors declare that they have no known competing financial interests or personal relationships that could have appeared to influence the work reported in this paper.

References

[1] U.S. Energy Information Administration (EIA). Electric Power Annual 2018. 2019.

[2] U.S. Energy Information Administration (EIA). U.S. natural gas-fired combined-cycle capacity surpasses coal-fired capacity 2019. https://www.eia.gov/todayinenergy/detail.php?id=39012.

[3] Reddy PJ. Clean Coal Technologies for Power Generation. CRC Press; 2014.

[4] International Energy Agency. Electricity Information 2019. 2019.

[5] Breeze P. Power Generation Technologies. 3rd ed. Elsevier; 2019.

[6] Mom AJA. Introduction to gas turbine. In: Jansohn P, editor. Mod. gas turbine Syst., Woodhead Publishing; 2013.

[7] Chiong MC, Chong CT, Ng J-H, Lam SS, Tran M-V, Chong WWF, et al. Liquid biofuels production and emissions performance in gas turbines : A review. Energy Convers Manag 2018;173:640–58.

[8] Seljak T, Pavalec K, Buffi M, Valera-Medina A, Katrasnik T, Chiaramonti D. Challenges and Solutions for Utilization of Bioliquids in Microturbines. J Eng Gas Turbines Power 2019;141:031401.

[9] Cammarota F, Benedetto A Di, Sarli V Di, Salzano E. The Effect of Hydrogen addition on the Explosion of Ethanol / Air Mixtures. Chem Eng Trans 2012;26:405–10.

[10] Di Benedetto A, Sanchirico R, Di Sarli V. Effect of pressure on the flash point of various fuels and their binary mixtures. Process Saf Environ Prot 2018;116:615–20.

[11] Agwu O, Valera-Medina A. Diesel/syngas co-combustion in a swirl-stabilised gas turbine combustor. Int J Thermofluids 2020;3–4:100026.

[12] Kurji H, Valera-Medina A, Okon A, Chong CT. Combustion and emission performance of

CO2/CH4/biodiesel and CO2/CH4/diesel blends in a Swirl Burner Generator. Energy Procedia 2017;142:154–9.

[13] Jiang L, Agrawal AK. Combustion of straight glycerol with / without methane using a fuel-flexible , low-emissions burner. Fuel 2014;136:177–84.

[14] Queiros P, Costa M, Carvalho RH. Co-combustion of crude glycerin with natural gas and hydrogen. Proc Combust Inst 2013;34:2759–67.

[15] Altaher MA, Li H, Andrews G. Co-firing of Kerosene and Biodiesel with Natural Gas in a Low NOx Radial Swirl Combustor. Proc. ASME Turbo Expo 2012, Copenhagen, Denmark: ASME (GT2012-68597); 2012.

[16] Chong CT, Chiong M-C, Ng J-H, Tran M-V, Valera-Medina A, Józsa V, et al. Dual-Fuel Operation of Biodiesel and Natural Gas in a Model Gas Turbine Combustor. Energy & Fuels 2020.

[17] U.S. Department of Energy. Clean Cities Alternative Fuel Price Report. 2019.

[18] Lefebvre AH, Ballal DR. Gas Turbine Combustion: Alternative Fuels and Emissions. 3rd ed. CRC Press; 2010.

[19] Wang S, Yang V, Hsiao G, Hsieh SY, Mongia HC. Large-eddy simulations of gas-turbine swirl injector flow dynamics. J Fluid Mech 2007;583:99–122.

[20] Kim HS, Arghode VK, Linck MB, Gupta AK. Hydrogen addition effects in a confined swirl-stabilized methane-air flame. Int J Hydrogen Energy 2009;34:1054–62.

[21] Kim HS, Arghode VK, Gupta AK. Flame characteristics of hydrogen-enriched methane-air premixed swirling flames. Int J Hydrogen Energy 2009;34:1063–73.

[22] Bhimani S, Alvarado JL, Annamalai K, Marsh C. Emission characteristics of methanol-in-canola oil emulsions in a combustion chamber. Fuel 2013;113:97–106.

[23] Bazooyar B, Shariati A, Hashemabadi SH. Characterization and Reduction of NO during the Combustion of Biodiesel in a Semi-industrial Boiler. Energy and Fuels 2015;29:6804–14.

[24] Bazooyar B, Hashemabadi SH, Shariati A. NOx formation of biodiesel in utility power plant boilers; Part B. Comparison of NO between biodiesel and petrodiesel. Fuel 2016;182:323–32.

[25] Ti S, Chen Z, Li Z, Xie Y, Shao Y, Zong Q, et al. Influence of different swirl vane angles of over fire air on flow and combustion characteristics and NOx emissions in a 600MWe utility boiler. Energy 2014;74:775–87.

[26] Wang Q, Chen Z, Che M, Zeng L, Li Z, Song M. Effect of different inner secondary-air vane angles on combustion characteristics of primary combustion zone for a down-fired 300-MWe utility boiler with overfire air. Appl Energy 2016;182:29–38.

[27] Sung Y, Choi G. Non-intrusive optical diagnostics of co- and counter-swirling flames in a dual swirl pulverized coal combustion burner. Fuel 2016;174:76–88.

[28] González-Cencerrado A, Gil A, Peña B. Characterization of PF flames under different swirl conditions based on visualization systems. Fuel 2013;113:798–809.

[29] Abdelaal MM, Hegab AH. Combustion and emission characteristics of a natural gas-fueled diesel engine with EGR. Energy Convers Manag 2000;64:301–12.

[30] Pirouzpanah V, Sarai RK. Reduction of emissions in an automotive direct injection diesel engine dual-fuelled with natural gas by using variable exhaust gas recirculation. Proc Inst Mech Eng Part D J Automob Eng 2003;217:719–25.

[31] Valera-Medina A, Syred N, Griffiths A. Visualisation of isothermal large coherent structures in a swirl burner. Combust Flame 2009;156:1723–34.

[32] Vigueras-Zuniga MO, Valera-Medina A, Syred N, Bowen P. High Momentum Flow Region and Central Recirculation Zone Interaction in Swirling Flows. Ing Mec Technol Y Desarro 2014;4:195–204.

[33] Chong CT, Hochgreb S. Spray combustion characteristics of palm biodiesel. Combust Sci Technol 2012;184:1093–107.

[34] Wardana ING, Widodo A, Wijayanti W. Improving Vegetable Oil Properties by Transforming Fatty Acid Chain Length in Jatropha Oil and Coconut Oil Blends. Energies 2018;11:394.

[35] Malaysia Energy Commission. Piped Gas Distribution Industry Statistics 2016. 2016.

[36] Hashimoto N, Nishida H, Ozawa Y. Fundamental combustion characteristics of Jatropha oil as alternative fuel for gas turbines. Fuel 2014;126:194–201.

[37] Imran S, Emberson DR, Diez A, Wen DS, Crookes RJ, Korakianitis T. Natural gas fueled compression ignition engine performance and emissions maps with diesel and RME pilot fuels. Appl Energy 2014;124:354–65.

[38] Evans MJ, Sidey JAM, Ye J, Medwell PR, Dally BB, Mastorakos E. Temperature and reaction zone imaging in turbulent swirling dual-fuel flames. Proc Combust Inst 2018;000:1–8.

[39] Sidey J, Mastorakos E. Visualisation of turbulent swirling dual-fuel flames. Proc Combust Inst 2017;36:1721–7.

[40] Bai XS, Fuchs L, Mauss F. Laminar Flamelet Structure at Low and Vanishing Scalar Dissipation Rate. Combust Flame 2000;120:285–300.

[41] Ahluwalia VK. Organic Chemistry: Fundamental Concepts. Alpha Science-International Ltd.; 2013.

[42] Elsamra RMI, Vranckx S, Carl SA. CH(A2) formation in hydrocarbon combustion: The temperature dependence of the rate constant of the reaction C2H + O2 -> CH(A2) + CO2. J Phys Chem A 2005;109:10287–93.

[43] Joklik RG, Daily JW, Pitz WJ. Measurements of CH radical concentrations in an acetylene/oxygen flame and comparisons to modeling calculations. Symp Combust 1988;21:895–904.

[44] Juchmann W, Latzel H, Shin DI, Peiter G, Dreier T, Volpp H-R, et al. Absolute Radical Concentration Measurements and Modeling of Low-Pressure CH4/O2/NO Flames. Proc Combust Inst 1998;27:469–76.

[45] Kojima J, Ikeda Y, Nakajima T. Basic aspects of OH(A), CH(A), and C2(d) chemiluminescence in the reaction zone of laminar methane-air premixed flames. Combust Flame 2005;140:34–45.

[46] Tomeczek J, Gradoń B. The role of N2O and NNH in the formation of NO via HCN in hydrocarbon flames. Combust Flame 2003;133:311–22.